This article has been accepted for inclusion in a future issue of this journal. Content is final as presented, with the exception of pagination.

Load Frequency Control of Power Systems With Electric Vehicles and Diverse Transmission Links Using Distributed Functional Observers

Thanh Ngoc Pham, Hieu Trinh, and Le Van Hien

***Abstract*—This paper presents a load frequency control scheme using electric vehicles (EVs) to help thermal turbine units to provide the stability fluctuated by load demands. First, a general framework for deriving a state-space model for general power system topologies is given. Then, a detailed model of a four-area power system incorporating a smart and renewable discharged EVs system is presented. The areas within the system are interconnected via a combination of alternating current/high voltage direct current links and thyristor controlled phase shifters. Based on some recent development on functional observers, novel distributed functional observers are designed, one at each local area, to implement any given global state feedback controller. The designed observers are of reduced order and dynamically decoupled from others in contrast to conventional centralized observer (CO)-based controllers. The proposed scheme can cope better against accidental failures than those CO-based controllers. Extensive simulations and comparisons are given to show the effectiveness of the proposed control scheme.**

***Index Terms*—Distributed functional observers (DFOs), high voltage direct current links, linear functional observers (LFOs), load frequency control (LFC), state observers, thyristor controlled phase shifters (TCPSs), vehicle-to-grid (V2G).**

Nomenclature

LFC	Load frequency control.
EV	Electric vehicle.
AC	Alternating current.
HVDC	High voltage direct current.
TCPS	Thyristor controlled phase shifter.
FACT	Flexible alternating current transmission.
BESS	Battery energy storage system.
V2G	Vehicle-to-grid.
LRO	Luenberger reduced-order observer.
LFO	Linear functional observer.
CFO	Centralized functional observer.
CO	Centralized observer.
DFO	Distributed functional observer.
i	ith area, $i = 1, 2, \ldots, N$.
n_i	Number of local state variables for ith area.
q_i	Order of DFO for ith area.
M_i, D_i	Inertia constant, load damping coefficient.
f_i, R_i	Frequency deviation, governor droop characteristic.
α_{gi}, α_{ei}	Thermal turbine and EVs participation factors.
K_{gi}, T_{gi}	Speed governor gain and time constant.
K_{ri}, T_{ri}	Reheat gain and time constant.
K_{ti}, T_{ti}	Thermal turbine gain and time constant.
K_{ei}, T_{ei}	EVs gain and time constant.
K_{ij}, K_{sij}	Gain constants of HVDC and TCPS links.
T_{dci}, T_{sij}	Time constants of HVDC and TCPS links.
T_{ij}	Tie-line synchronizing coefficient.
ACE_i, b_i	Area control error, frequency bias constant.
P_{aci}, P_{dci}	Interchange ac and HVDC power.
$P_{\mathrm{ac},ij}$, P_{sij}	Incremental changes in ac tie-line and TCPS power.
$P_{\mathrm{tie},i}$, P_{li}	Tie-line power interchange deviation and local load demand.
P_{ei}, P_{gi}	Incremental changes in EVs and turbine output power.
P_{ri}	Incremental change in intermediate output of turbine.
X_{gi}	Incremental change in governor valve position.
P_{cgi}, P_{cei}	Thermal turbine and EVs control inputs.
P_{ci}	Local control input.

Manuscript received August 14, 2014; revised December 22, 2014, March 19, 2015, and May 14, 2015; accepted June 22, 2015. Paper no. TSG-00818-2014. *(Corresponding author: Hieu Trinh.)*

T. N. Pham is with the Centre for Intelligent Systems Research, Deakin University, Geelong, VIC 3217, Australia (e-mail: ntpham@deakin.edu.au).

H. Trinh is with the School of Engineering, Deakin University, Geelong, VIC 3217, Australia (e-mail: hieu.trinh@deakin.edu.au).

L. V. Hien is with the Department of Mathematics, Hanoi National University of Education, Hanoi 84, Vietnam (e-mail: hienlv@hnue.edu.vn).

Color versions of one or more of the figures in this paper are available online at http://ieeexplore.ieee.org.

Digital Object Identifier 10.1109/TSG.2015.2449877

I. Introduction

LOAD FREQUENCY control (LFC) is paramount in the operation of interconnected power systems. Due to load disturbances, the total supplied power does not always match the power demand and this causes some undesirable effects [1], [2] such as the frequency and interchange power may widely oscillate and deviate from the scheduled values. Thus, the main objective of LFC is to maintain the frequency and interchange power at the desired values through appropriate control action [3]–[5].

A multi-area complex power system normally comprises a large number of distant or remote areas where each area is interconnected to others via ac power lines (see [4], [5]). Along with ac transmission, HVDC transmission is also used due to some economic benefits and its ability to enhance stability in the system. In general, HVDC transmission does not require reactive power compensation, has lower electrical loses and is more economical when electric power is transferred over long distances (see [2], [6], [7]). By using ac and HVDC links together, better stability margin and dynamic performance can be achieved (see [8]–[10]). On the other hand, TCPS which is an application FACT, is another possible tool for enhancing the dynamic performance of the system [11]. TCPS located along an ac tie-line can regulate power flow by changing the relative voltage angle between the two interconnected areas [12].

Recently, EV has attracted considerable research interests due to its environmentally friendly characteristics such as lower greenhouse emission and noise pollution [13], [14]. Notably, EV has its own battery and with the V2G technology, a fleet of thousands of EVs can be used as controllable energy storage devices to participate in power system operation [15], [16]. Operating as a large BESS, a fleet of EVs is very effective in stabilizing load and frequency fluctuations (see [17]–[21]) due to the fast response characteristics of EVs battery [22]. Furthermore, hundred thousands of EVs can be connected to the grid as a large power plant. This situation is feasible since most of EVs are plug-in to the grid when parking at station or at home [23]. Therefore, it is possible that EVs participate in the LFC to assist power units to rapidly suppress load fluctuations [23]–[26]. EVs interact to grid by bidirectional power electronic devices so that they react to the new load set-point faster than conventional generators [26]. In order to group a fleet of thousands of EVs, the concept of aggregator has been developed [16], [24], [25], [27]–[30]. Here, the role of an aggregator is to gather and send information about the EVs' status to the control center and reallocate the control command to disperse EVs. To develop a smart power grid that can integrate EVs, an open communication infrastructure such as network control system or wide-area communication is necessary. With this communication infrastructure, EVs receive control signals and update in real-time their data information such as the state of charge, capacity of EVs' power and the number of connected EVs to the grid [16], [23]–[30]. The communication infrastructure for EVs comprises power line communication, general packet radio service, an Internet connection [22], [24], [28], [29], wireless protocol with ZigBee technology, and Bluetooth [16]. In this paper, we consider that most of EVs at each local area are parked at stations which are closed together and the communication happens at a very high speed relative to the speed of the closed-loop system. Therefore, we ignore any network-induced communication delay that may arise in the communication channel. Such an assumption is reasonable and it will be justified later on in this paper.

In this paper, we present a novel LFC scheme that incorporates EVs into the stabilization of load fluctuations. To demonstrate the feasibility of our scheme, we consider a four-area power system where each area is interconnected to others via a combination of ac/HVDC links and TCPS. A detailed mathematical model of a four-area power system including the dynamics of EVs is derived in this paper. Accordingly, with the availability of a detailed mathematical model, a state feedback control law can be easily designed to optimally determine the charging/discharging behaviors of EVs and the generating units' power output. However, any feasible optimal state feedback control law inevitably requires the information of all the state variables in order to generate a control input signal [4]. Hence, it becomes unrealistic if some state variables are not available for feedback control. To overcome this problem, conventional CO-based controllers where state observers were used to reconstruct the unmeasured states [31], [32] have been proposed. However, CO-based control schemes require complex hardware and a central facility for processing very large amount of information in real-time and on-line. Therefore, to be able to implement any optimally designed global state feedback control law, it is important to develop some reduced-order distributed observer-based schemes where the processing of information and the control task are shared among the local controllers. For security and economical considerations, it is desirable that these controllers share as little information among themselves as possible.

On the other hand, LFOs estimate linear functions of the state vector without estimating all the individual states and so reduce the order and complexity of the designed observers [33]. The significance of this is that any designed state feedback control law can now be implemented by using a minimum-order LFO leading to a simpler way to implement a state feedback control law. Indeed, for large complex systems such as multi-area power systems, LFOs have a vast potential to reduce the cost, weight, volume of engineered systems and simplify their maintenance and installation. In this paper, based on some recent development on LFOs [33]–[37], we design DFOs, one at each local area, in order to carry out the practical implementation of any given (designed) global state feedback control law. The control input signal can be reconstructed as the functional state variables. The proposed observers are of reduced-order, dynamically decoupled from others and therefore the proposed scheme is simple to implement. Recently, LFC using functional observers has been reported in [38], but for a simple model of a two-area interconnected power system. In contrast, in this paper, EVs are used to help thermal turbine units to provide the stability fluctuated by load demands. We lay down the foundation for deriving a state-space model for general power system topologies with diverse transmission links (i.e., ac/HVDV, TCPS) and EVs. For the first time, the derived state-space model contains the dynamic interactions of EVs and how they effect the global stability of the infrastructure. We provide an in-depth LFC of a complex four-area power system incorporating EVs in each area and the areas themselves are interconnected by a diverse transmission links of ac/HVDC and integrated TCPS. We also show that the design method can deal with general power systems with diverse links, topologies and a large number of connected areas. We validate this by showing further studies on five- and six-area interconnected power systems.

II. Multi-Area Interconnected Power Systems

Fig. 1 shows a general transfer function model of N-area interconnected power system arising from the original

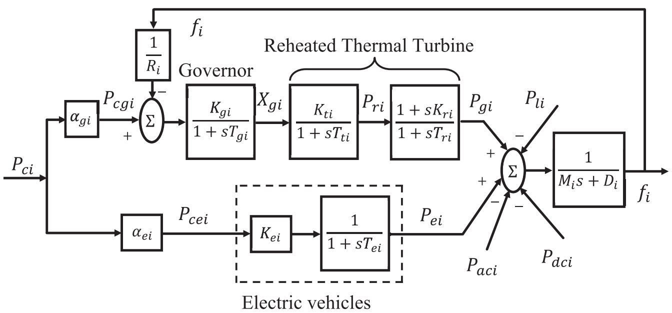

Fig. 1. Transfer function model of N-area interconnected power system.

model [39]. In this paper, the following considerations are added to the model: 1) a dynamics model for the discharging of EVs; 2) plants with reheated thermal turbines; 3) HVDC links, represented in the model by P_{dci}; and 4) TCPS in ac power tie-lines, represented in the model by P_{aci}.

In order to maintain system frequency and power tie-line at the scheduled values, the control center sends the incremental change in power set-point, P_{ci}, and through participation factors α_{gi} and α_{ei}, control signals P_{cgi} and P_{cei} are sent to regulate the power output of the generating units and EVs, respectively. The bidirectional power electronic devices allow EVs to pump energy into the grid and their power capacity can be contributed to the LFC control as power plant. The aggregator collects information on all EVs and provides them to the control center. In addition, the aggregator receives the power set-point from the control center and then allocates it to dispersed EVs. The fleet of EVs is modeled [17]–[20] by a first-order with time constant T_{ei} and gain K_{ei}. From Fig. 1, the EVs output power deviation is

$$P_{ei}(s) = \frac{K_{ei}}{1+sT_{ei}} P_{\text{cei}}(s). \tag{1}$$

In order to participate HVDC links into LFC, the supplemental HVDC proportional controller is implemented. The HVDC power interchange, P_{dci}, of area i is determined by the HVDC control signal $\mathcal{E}_i$ with a time constant T_{dci} [8]–[10], [40]. The $\mathcal{E}_i$ signal is computed according to the difference between the frequency deviations of area i and the other areas j, $j = 1, 2, \ldots, N, j \neq i$ [41] with a HVDC gain K_{ij}. Hence, P_{dci} is obtained, where

$$P_{\text{dci}}(s) = \frac{1}{1+sT_{\text{dci}}} \mathcal{E}_i(s) \tag{2}$$

where $\mathcal{E}_i(s) = \sum_{j=1, j\neq i}^{N} K_{ij}(f_i(s) - f_j(s))$. Note that $K_{ij} = 0$ when there is no HVDC link between areas i and j.

Without TCPS, the ac power tie-line deviation between areas i and j is given according to [39]

$$P_{\text{ac},ij}(s) = \frac{2\pi}{s} T_{ij}\big(f_i(s) - f_j(s)\big). \tag{3}$$

With integrated TCPS, the ac power tie-line deviation between areas i and j is obtained as [11]

$$P_{\text{ac},ij}(s) = \frac{2\pi}{s} T_{ij}\big(f_i(s) - f_j(s)\big) + P_{sij}(s) \tag{4}$$

where $P_{sij}(s)$ is the TCPS power deviation and it is defined as

$$P_{sij}(s) = T_{ij} \frac{K_{sij}}{1+sT_{sij}} f_i(s). \tag{5}$$

Therefore, the ac tie-line power interchange deviation at area i is obtained, where

$$P_{\text{aci}}(s) = \sum_{j=1, j\neq i}^{N} P_{\text{ac},ij}(s). \tag{6}$$

In LFC, it is important to maintain zero steady-state error for tie-line power and frequency deviations when the system is subjected to any step load disturbance. The deviations from these scheduled values are combined and represented in the ACE. Within each area, the ACE is computed according to the following:

$$\text{ACE}_i(t) = P_{\text{tie},i}(t) + b_i f_i(t) \tag{7}$$

where $P_{\text{tie},i}(t) = P_{\text{aci}}(t) + P_{\text{dci}}(t)$ is the tie-line power interchange deviation at area i. For an N-area interconnected power system, note that $\sum_{i=1}^{N} P_{\text{tie},i}(t) = 0$. Zero steady-state error is achieved if all ACE_i $(i = 1, 2, \ldots, N)$ are forced to have zero steady-state value in response to any step load disturbance. This implies that a successful LFC scheme needs to include integral controllers, the inputs to which are the ACEs.

Accordingly, for the multi-area power system as shown in Fig. 1, a state-space model for each local area can be derived as follows:

$$\begin{aligned}\dot{x}_i(t) = A_{ii}x_i(t) &+ \sum_{j=1, j\neq i}^{N} A_{ij}x_j(t) + B_i u_i(t)\\ &+ \Gamma_i d_i(t), \quad i = 1, 2, \ldots, N\end{aligned} \tag{8}$$

where $x_i(t) \in \mathbb{R}^{n_i}$, $u_i(t) = P_{ci}(t)$ and $d_i(t) = P_{li}(t)$ are the local state vector, local control input and local load disturbance, respectively. The local state vector for each area, $x_i(t) \in \mathbb{R}^{n_i}$, is defined as follows:

$$\begin{aligned}x_i(t) = \big[&f_i(t) \quad X_{gi}(t) \quad P_{ri}(t) \quad P_{gi}(t) \quad P_{ei}(t)\\ &\textstyle\int \text{ACE}_i(t)dt \quad P_{\text{tie},i}(t) \quad P_{\text{dci}}(t) \quad P_{sij}(t)\big]^T.\end{aligned} \tag{9}$$

In this paper, we define the outputs at each local area $y_i(t) \in \mathbb{R}^5$ to be

$$\begin{aligned}y_i(t) &= \left[P_{\text{tie},i}(t) \quad f_i(t) \quad X_{gi}(t) \quad P_{gi}(t) \quad \int \text{ACE}_i(t)dt\right]^T\\ &= C_i x(t).\end{aligned} \tag{10}$$

Even though the main results of this paper can be applied to general power system topologies with a large number ($N >> 2$) of connected areas. However, for ease of presentation, we consider a four-area power system with EVs and various types of ac/HVDC links and TCPS. The topology of the system is depicted in Fig. 2. This model is quite practical and large enough to demonstrate our distributed control scheme. Based on the development given in (1)–(10), the following state-space model is obtained:

$$\dot{x}(t) = Ax(t) + Bu(t) + \Gamma d(t) \tag{11}$$

where $x(t) \in \mathbb{R}^{31}$, $u(t) \in \mathbb{R}^4$, and $d(t) \in \mathbb{R}^4$ are the global state vector, control vector, and load disturbance

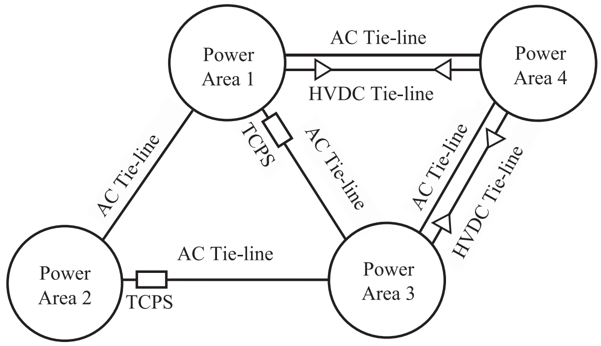

Fig. 2. Block diagram representation of a four-area power system.

vector, respectively. Here, $x(t)$ comprises local state vectors of the four areas, where $x(t) = [x_1^T(t)\ x_2^T(t)\ x_3^T(t)\ x_4^T(t)]^T$. The global control input vector, $u(t)$, comprises four local control inputs, where $u(t) = [P_{c1}(t)\ P_{c2}(t)\ P_{c3}(t)\ P_{c4}(t)]^T$, and $d(t)$ comprises four local load disturbances, where $d(t) = [P_{l1}(t)\ P_{l2}(t)\ P_{l3}(t)\ P_{l4}(t)]^T$. The local state vector for each area, $x_i(t)$, is defined as $x_i(t) = [x_{i1}^T(t)\ \ x_{i2}^T(t)]^T$, where $x_{i1}(t) = [f_i(t)\ \ X_{gi}(t)\ \ P_{ri}(t)\ \ P_{gi}(t)\ \ P_{ei}(t)\ \ \int \mathrm{ACE}_i(t)dt]^T$ and $x_{i2}(t)$ is defined as $x_{12}(t) = [P_{\mathrm{tie},1}(t)\ P_{\mathrm{dc}1}(t)\ P_{s13}(t)]^T$, $x_{22}(t) = [P_{\mathrm{tie},2}(t)\ \ P_{s23}(t)]^T$, $x_{32}(t) = [P_{\mathrm{tie},3}(t)\ \ P_{\mathrm{dc}3}(t)]^T$ and $x_{42}(t) = [\emptyset]$. In (11), $B = \text{block} - \text{diag}(B_1, B_2, B_3, B_4)$, $\Gamma = \text{block} - \text{diag}(\Gamma_1, \Gamma_2, \Gamma_3, \Gamma_4)$ and

$$A = \begin{bmatrix} A_{11} & A_{12} & A_{13} & A_{14} \\ A_{21} & A_{22} & A_{23} & A_{24} \\ A_{31} & A_{32} & A_{33} & A_{34} \\ A_{41} & A_{42} & A_{43} & A_{44} \end{bmatrix}.$$

Please refer to Appendix A for a detailed description of the matrices $A \in \mathbb{R}^{31\times31}$, $B \in \mathbb{R}^{31\times4}$, and $\Gamma \in \mathbb{R}^{31\times4}$.

III. Global State Feedback Control Law and Some Issues Associated With its Implementation

In (11), the integrals of all the ACEs are used as controlled feedback variables to guarantee zero steady-state for the net power interchange and frequency to any step load change. Therefore, the requirement on the system stability and closed-loop control performance can be achieved by adopting the global policy for controller design. In this regard, well established principles of pole-placement or optimal state feedback control have been extensively covered. Thus, let us now assume that a global stabilizing state feedback control law of the form $u(t) = Fx(t)$, $F \in \mathbb{R}^{4\times31}$, can be designed to satisfy some prescribed closed-loop system performance. Please refer to Appendix B for the data used in the analysis and design of controller and distributed observers in this paper.

Figs. 3 and 4 show the responses of the net power interchange and frequency deviation of area 1 when a 0.1 p.u. step load change occurred at area 1. As mentioned in Section I, TCPS and HVDC can enhance stability of the system, and this can be clearly seen in Figs. 3 and 4. It is also clear from the figures that the designed global state feedback controller effectively stabilizes the closed-loop system with acceptable transient responses and zero steady-state deviations. Also, Fig. 5 shows the contribution of EVs and reheated thermal turbine to LFC with their participation factors 0.1 and 0.9, respectively.

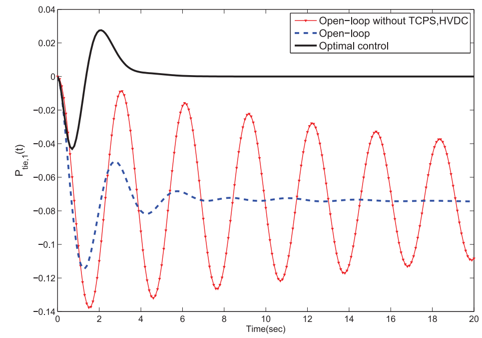

Fig. 3. $P_{\mathrm{tie},1}(t)$ responses to a 0.1 p.u. step load change at area 1.

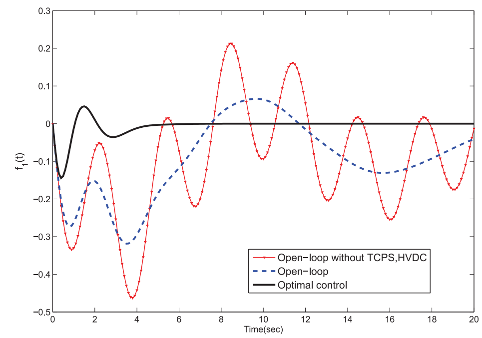

Fig. 4. $f_1(t)$ responses to a 0.1 p.u. step load change at area 1.

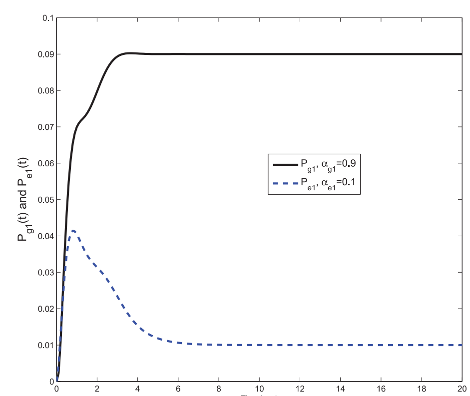

Fig. 5. $P_{g1}(t)$ and $P_{e1}(t)$ responses to a 0.1 p.u. step load change at area 1.

As can be seen from Fig. 5, the EVs and thermal turbine able to provide the required 0.1 p.u. power load demand to area 1.

Let us now turn our attention to the implementation of the global state feedback controller. For this, let us express $u(t)$ as follows:

$$u(t) = \begin{bmatrix} u_1(t) \\ \vdots \\ u_4(t) \end{bmatrix} = \begin{bmatrix} F_1 \\ \vdots \\ F_4 \end{bmatrix} x(t) \tag{12}$$

where $F_i \in \mathbb{R}^{1\times31}$ is the feedback gain matrix of the ith area. Thus, the control law for each area is given as $u_i(t) = F_i x(t)$. Also, let us partition F_i as $F_i = \begin{bmatrix} F_{i1}\ F_{i2}\ F_{i3}\ F_{i4} \end{bmatrix}$. Hence

$$u_i(t) = \sum_{j=1}^{4} u_{ij}(t) \tag{13}$$

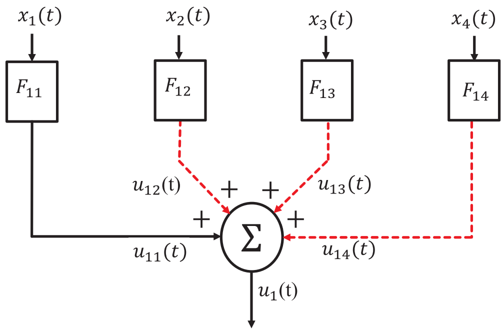

Fig. 6. Block-diagram implementation of control signal $u_1(t)$ for area 1.

where $u_{ij}(t) = F_{ij}x_j(t)$. Fig. 6 shows a block-diagram implementation of the control signal $u_1(t)$ for area 1. The dashed (red) lines represent control signals $u_{1j}(t)$, constructed at areas 2, 3, 4 and they are sent over to area 1 to form an overall control signal for $u_1(t)$. Clearly, the critical problem with this control law is the unavailability of some of the state variables for feedback control purpose. In addition, due to the global nature of the feedback control law, it requires data transfer as depicted by the dashed (red) lines in Fig. 6. As discussed in the introduction section, conventional CO-based controllers where Luenberger-type state observers have been employed to reconstruct the unmeasured states [31]–[32]. However, the main problem with this approach is that the order of the designed state observers is still very high, especially for the four-area interconnected power system under studied in this paper. In Section I, we have highlighted the importance and the need for developing some reduced-order distributed observer-based control schemes where the processing of information and the control task are shared among the local control stations.

In the next section, we will discuss the design of some novel DFOs to overcome or lessen some of the issues associated with CO-based schemes. We will show that the incorporation of LFOs into LFC of multi-area interconnected power systems will lead to a simpler control scheme and increased overall system reliability and practicality.

IV. Distributed Functional Observers for Interconnected Power Systems

It is clear that the control input into each local power area, $u_i(t) = F_i x(t)$, is a linear function of the global state vector $x(t)$. Thus, it would make more sense to design a reduced-order LFO to directly generate the estimate $\hat{u}_i(t)$ than to design a reduced-order Luenberger state observer (LRO) to estimate $x(t)$ and hence $\hat{u}_i(t) = F_i\hat{x}_i(t)$. As pointed out in [31], [32], and [38], when the load disturbance is a step-change of any magnitude, $d(t)$ can be ignored altogether in the design of state observers and the resulting observer-based closed-loop system still ensures zero steady-state values for tie-line power and frequencies. In this section, based on some recent development on LFOs [33]–[37], we design DFOs where they are dynamically decoupled from each others while at the same time ensuring that the LFC task is shared among them. Now, to design an LFO to estimate any given linear function of the state vector, $z_i(t) = F_i x(t)$ $(i = 1, 2, 3, 4)$, where $F_i \in \mathbb{R}^{1\times 31}$ is any given matrix, let us consider the following reduced-order observer for each area:

$$\begin{aligned}\hat{z}_i(t) &= K_i w_i(t) + E_i y_a^i(t),\ i = 1, 2, 3, 4\\ \dot{w}_i(t) &= \Lambda_i w_i(t) + G_i u_i(t) + J_i y_a^i(t)\end{aligned}\tag{14}$$

where $w_i(t) \in \mathbb{R}^{q_i}$, K_i, E_i, Λ_i, G_i, and J_i are observer parameters to be determined such that $\hat{z}_i(t)$ converges to $z_i(t)$ with any prescribed convergence rate.

In (14), $y_a^i(t)$ denotes the augmented output vector which must be used at the ith area in order to reconstruct $z_i(t)$. The composition of $y_a^i(t)$ will be discussed in more details a bit later on. Note that from (14), each observer is completely decoupled from each other as there is no link between $w_i(t)$ and $w_j(t)$, $j \neq i$. This is in contrast to the centralized Luenberger-based controller which needs to send the control signals from the central facility to all different areas. From the viewpoint of practical and ease of implementation, it is most desirable that $y_a^i(t)$ contains only the local output information, i.e., $y_a^i(t) = y_i(t) = C_i x(t)$. In such case, the observer is a complete decentralized observer as there is no exchange of information among the areas. However, this is not possible since the matrix pair (A, C_i) is not observable nor the triplet (A, C_i, F_i) is functional observable according to the functional observability test [36]. What this means is that there does not exist any state observer nor functional observer if only the local output information, $y_i(t)$, is used to reconstruct $z_i(t)$. Thus, let

$$y_a^i(t) = \begin{bmatrix} y_i(t)\\ y_r^i(t)\end{bmatrix} = \begin{bmatrix} C_i\\ C_r^i\end{bmatrix} x(t) = C_a^i x(t)\tag{15}$$

where $C_a^i \in \mathbb{R}^{p_i\times n}$. Here, $y_r^i(t)$ denotes the additional outputs from the other remote areas and they are sent over to the ith area. These outputs should be selected so that at least the triplet (A, C_a^i, F_i) is functional observable. Ignoring $d(t)$ and let us rearrange (11) and together with (15), we have

$$\begin{aligned}\dot{x}(t) &= Ax(t) + \tilde{B}_i u_i(t) + \tilde{B}_r u_r(t)\\ y_a^i(t) &= C_a^i x(t)\end{aligned}\tag{16}$$

where $u_r(t) \in \mathbb{R}^3$ contains the three remote control inputs of the three remote power areas, and $\tilde{B}_r \in \mathbb{R}^{31\times 3}$. Define the following error vectors:

$$\varepsilon_i(t) = w_i(t) - L_i x(t),\ \ e_i(t) = \hat{z}_i(t) - z_i(t)\tag{17}$$

hence

$$e_i(t) = K_i\varepsilon_i(t) + \left(K_i L_i + E_i C_a^i - F_i\right)x(t)\tag{18}$$

where $\varepsilon_i(t) \in \mathbb{R}^{q_i}$, $e_i(t) \in \mathbb{R}$, and $L_i \in \mathbb{R}^{q_i\times n}$. We take the derivative of $\varepsilon_i(t)$ as $\dot{\varepsilon}_i(t) = \dot{w}_i(t) - L_i\dot{x}(t)$. Using (16)–(18), we have

$$\begin{aligned}\dot{\varepsilon}_i(t) = \Lambda_i\varepsilon_i(t) &+ \left(\Lambda_i L_i + J_i C_a^i - L_i A\right)x(t)\\ &+ \left(G_i - L_i\tilde{B}_i\right)u_i(t) - L_i\tilde{B}_r u_r(t).\end{aligned}\tag{19}$$

From (18) and (19), the error $e_i(t)$ converges asymptotically to zero for any initial condition $w_i(0)$

This article has been accepted for inclusion in a future issue of this journal. Content is final as presented, with the exception of pagination.

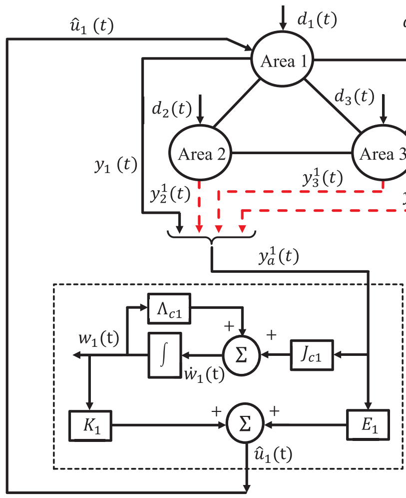

Fig. 7. Block-diagram implementation of a DFO for area 1.

and any $u_i(t)$ if the following matrix equations are satisfied:

$$\Lambda_i L_i + J_i C_a^i - L_i A = 0,\ \Lambda_i \text{ is Hurwitz} \tag{20}$$
$$F_i - K_i L_i - E_i C_a^i = 0 \tag{21}$$
$$L_i \tilde{B}_r = 0 \tag{22}$$
$$G_i = L_i \tilde{B}_i. \tag{23}$$

Furthermore, if the eigenvalues of matrix Λ_i can be assigned, then the error $e_i(t)$ converges with any prescribed convergence rate to zero.

Now, we propose to construct the estimated control signal of $u_i(t)$ according to the following law:

$$\hat{u}_i(t) = \hat{z}_i(t) = K_i w_i(t) + E_i y_a^i(t) \tag{24}$$

and hence the dynamics of the observer (14) is reduced to

$$\dot{w}_i(t) = \Lambda_{ci} w_i(t) + J_{ci} y_a^i(t) \tag{25}$$

where $\Lambda_{ci} = \Lambda_i + G_i K_i$ and $J_{ci} = J_i + G_i E_i$. Together, (24) and (25) now form an observer-based control scheme for the ith area. Fig. 7 shows a block-diagram implementation of the DFO for the power area 1.

Incorporating the above scheme (24)–(25) into the four areas of the power system, we obtain the following augmented closed-loop system:

$$\dot{x}(t) = A_c x(t) + \sum_{i=1}^{4} \tilde{B}_i K_i w_i(t) + \Gamma d(t)$$
$$\dot{w}_i(t) = \Lambda_{ci} w_i(t) + J_{ci} C_a^i x(t),\ \ i = 1, 2, 3, 4 \tag{26}$$

where $A_c = A + \sum_{i=1}^{4} \tilde{B}_i E_i C_a^i$.

By using (17) and (21), the first equation of (26) can be expressed as follows:

$$\dot{x}(t) = Ax(t) + \sum_{i=1}^{4} \tilde{B}_i (F_i - K_i L_i) x(t) + \sum_{i=1}^{4} \tilde{B}_i K_i w_i(t) + \Gamma d(t)$$
$$= (A + BF)x(t) + \sum_{i=1}^{4} \tilde{B}_i K_i \varepsilon_i(t) + \Gamma d(t). \tag{27}$$

Subject to the satisfaction of the matrix equations (20)–(23), from (18) and (19), we have

$$\dot{\varepsilon}_i(t) = \Lambda_i \varepsilon_i(t),\ e_i(t) = K_i \varepsilon_i(t),\ i = 1, 2, 3, 4 \tag{28}$$

which implies that the errors $\varepsilon_i(t)$ and $e_i(t)$ converge to zero given that matrix Λ_i is Hurwitz.

From (27) and (28), the following augmented closed-loop system is obtained:

$$\begin{bmatrix} \dot{x}(t) \\ \dot{\varepsilon}(t) \end{bmatrix} = \begin{bmatrix} (A + BF) & A_\varepsilon \\ 0 & \Lambda_\varepsilon \end{bmatrix} \begin{bmatrix} x(t) \\ \varepsilon(t) \end{bmatrix} + \Gamma d(t) \tag{29}$$

where

$$\varepsilon(t) = \begin{bmatrix} \varepsilon_1(t)^T & \varepsilon_2(t)^T & \varepsilon_3(t)^T & \varepsilon_4(t)^T \end{bmatrix}^T$$
$$A_\varepsilon = \begin{bmatrix} \tilde{B}_1 K_1 & \tilde{B}_2 K_2 & \tilde{B}_3 K_3 & \tilde{B}_4 K_4 \end{bmatrix}$$
$$\Lambda_\varepsilon = \text{block} - \text{diag}(\Lambda_1, \Lambda_2, \Lambda_3, \Lambda_4).$$

Clearly, the eigenvalues of the above augmented closed-loop system are the union of the eigenvalues of the optimal state feedback controller and of the DFOs. Since Λ_i is required to be Hurwitz and the controller stabilizes $(A + BF)$, the overall augmented closed-loop system is therefore stable. This proves that our DFO scheme obeys the separation principle. Thus, the remaining task is to solve for the unknown matrices Λ_i, L_i, K_i, E_i, J_i, and G_i such that (20)–(23) are satisfied. This task can be accomplished by employing an effective design algorithm reported in [33].

Now, we discuss the composition of $y_a^i(t)$ where it comprises the local output of the ith area, $y_i(t)$, as defined in (10), and additional outputs from the other areas denoted by $y_r^i(t)$. The local output $y_i(t)$ includes $P_{\text{tie},i}(t)$, $f_i(t)$, $X_{gi}(t)$, and $P_{gi}(t)$. Since $\text{ACE}_i(t)$ is as defined in (7) and with the availability of $P_{\text{tie},i}(t)$ and $f_i(t)$, $\int \text{ACE}_i(t)dt$ can be easily constructed at the ith area. The remote output variables, $y_r^i(t)$, can be systematically selected such that the ith area becomes functional observable. This is done by testing the rank condition of two existence conditions reported in [37, Th. 4.6]. Using this test, we have found that the minimal choice of $y_r^i(t)$ does not require any of the $P_{gj}(t)$ to be sent over to the ith area. Also, it is worthwhile to point out that the minimal choice of $y_r^i(t)$ does not necessarily provide a good outcome since there is a trade-off between the order of the designed DFOs and the number of available output variables.

Accordingly, a comprehensive analysis on the trade-off between the amount of exchanged information and the order of the designed DFOs has been carried out and the results are tabulated in Table I. Note that for the case where all the outputs of the local area, $y_i(t)$, and all the outputs of the three remote areas, $y_j(t)$, are available, this gives a total of 19 outputs. This case is tabulated in the first row of Table I. Accordingly, with 19 outputs and 31 state variables, a twelfth-order LRO is required, whereas a significantly lower order of fifth-order CFO is required. On the other hand, the resulting order of the designed DFOs is only a second-order for each power area. Here, four dynamically decoupled functional observers, one at each area, and each of only a second-order can be used to implement the global control law.

Extensive simulation has been carried to test the performance of the designed DFOs. For illustrative purpose,

TABLE I
MINIMUM ORDER OBSERVER ANALYSIS

Outputs	LRO orders	CFO orders	DFO orders			
			Area 1	Area 2	Area 3	Area 4
19	12	5	2	2	2	2
18	13	6	3	3	3	3
17	14	7	5	5	5	5
16	15	8	7	7	7	7
15	16	9	Does not exist			
18: one of the three remote signals $P_{gj}(t)$ is not sent over						
17: two of the three remote signals $P_{gj}(t)$ are not sent over						
16: all three remote signals $P_{gj}(t)$ are not sent over						
15: all three remote signals $P_{gj}(t)$ are not sent over, and any one of the remote signals $X_{gi}(t)$ is not sent over						

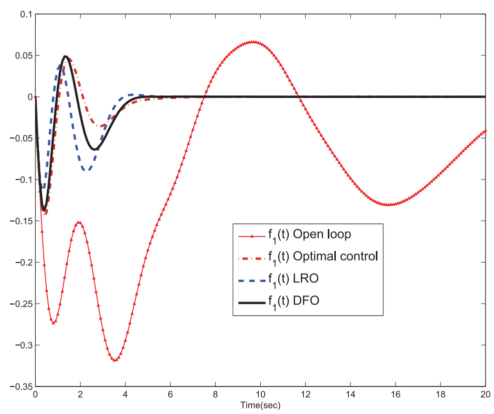

Fig. 8. $f_1(t)$ responses to a 0.1 p.u. step load change at area 1.

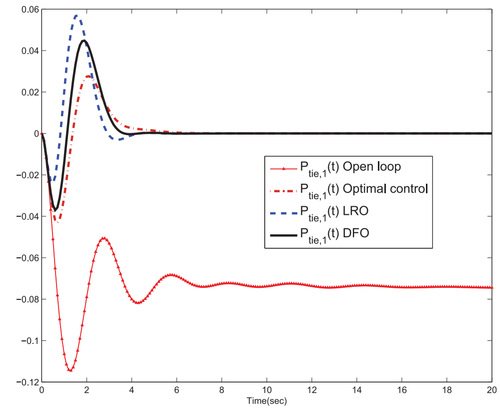

Fig. 9. $P_{\text{tie},1}(t)$ responses to a 0.1 p.u. step load change at area 1.

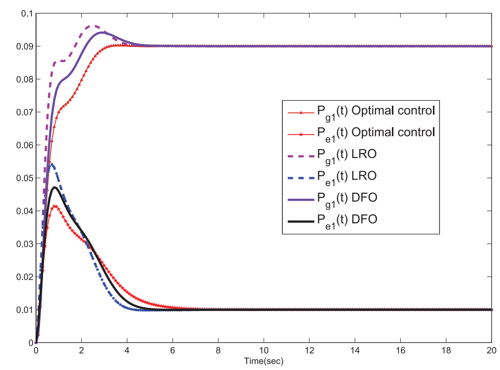

Fig. 10. $P_{g1}(t)$ and $P_{e1}(t)$ responses to a 0.1 p.u. step load change at area 1.

Figs. 8 and 9 show simulations of the performance of DFOs and LRO. Clearly, both observer-based control strategies can bring the steady-state output of the frequency deviation and the power tie-line to zero and with satisfactory transient performance as evident from the figures. As we have already stated in this paper, the proposed DFOs obey the separation principle as is the case for the LRO-based control design. The primary advantage of having a reduced-order closed-loop system is realized with the proposed DFOs observer-based control strategy. For the considered example, the functional observer-based control strategy uses four second-order controllers, each with assigned poles at $(-2, -3)$, in comparison to the twelfth-order centralized LRO. Note that these DFOs are located in their respective areas, and therefore the control signals need not be sent from one area to another.

Fig. 10 shows the contribution of EVs and reheated thermal turbine to LFC with their participation factors 0.1 and 0.9, respectively. As can be seen from Fig. 10, both the DFOs and the LRO able to provide the required 0.1 p.u. power load demand to area 1.

Remark 1: We have undertaken more simulations to show the effect of Q, R, and α on the transient responses of the closed-loop system under various optimal state feedback controllers. For this, we consider three scenarios as tabulated in Table II. Note that scenario A_1 is the one considered in Appendix B. Scenarios A_2 and A_3 consider two cases where the value in matrices Q and R is reduced, respectively. While scenario A_4 considers the case where α is reduced to a smaller value. As can be seen from Fig. 11, changing Q and R effects the transient responses of the closed-loop system. While a smaller $|\alpha|$ leads to a longer settling time, as expected. Indeed, these observations are consistent with the well-established theory of linear quadratic regulator (LQR) design.

Note that, one of the key objectives in this paper is to present a new framework for distributed implementation, using novel DFOs, of any designed state feedback control law $u(t) = Fx(t)$. Therefore, with our method, for any given state feedback controller we can readily design DFOs to realize the implementation of such controller. To further illustrate this point, we have designed three set of DFOs corresponding to the three optimal state feedback controllers as presented in scenarios A_2, A_3, A_4. Extensive simulations have been conducted. For illustrative purpose, Fig. 12 shows that the performance of our DFO-based controller compared well to that of the optimal state feedback controller. Hence, demonstrating the effectiveness of our DFO scheme.

We have also undertaken simulations for cases where sudden load changes occurred in two (or more) areas at once and with different amplitudes. For this, we consider two scenarios as tabulated in Table III. Fig. 13 shows the response of the frequency deviation $f_1(t)$ of area 1 for scenario B_2. It is clear from the figure and as expected, the frequency deviation $f_1(t)$ at area 1 converges to zeros and with satisfactory transient response.

Remark 2: Some critical events such as faulty controller components, accidental failures, or even some deliberate acts

This article has been accepted for inclusion in a future issue of this journal. Content is final as presented, with the exception of pagination.

TABLE II
DIFFERENT VALUES OF Q, R, AND α

Scenarios	Q	R	α
A_1	I_{31}	I_4	-1
A_2	$0.1 \times I_{31}$	I_4	-1
A_3	I_{31}	$0.2 \times I_4$	-1
A_4	I_{31}	I_4	-0.3

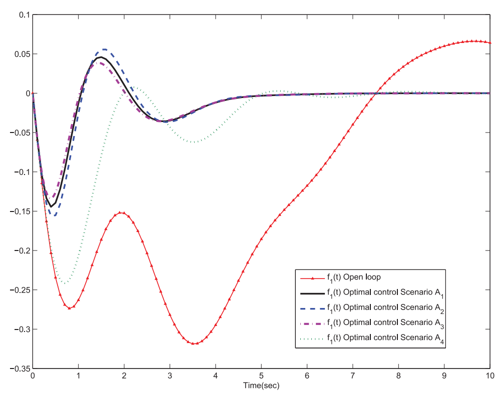

Fig. 11. $f_1(t)$ responses to a 0.1 p.u. step load change at area 1 for scenarios A_1–A_4.

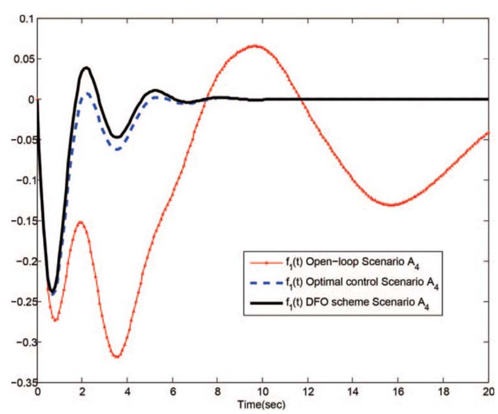

Fig. 12. $f_1(t)$ responses to a 0.1 p.u. step load change at area 1 for scenario A_4.

of vandalism may cause a complete shutdown of some local controllers and as a result, led to loss of control signals. We can demonstrate that our DFO scheme is more robust against loss of control signals than CO-based control schemes. Indeed, in those CO-based control schemes, the tasks of processing information, estimation and control are done at the central control facility. Hypothetically, if the control signals are lost due to a complete shutdown of the central control facility, then those CO-based control schemes would cease to operate. In contrast, if there are some failures to one or some of the local controllers, we still have some remaining controllers properly functioned. Thus, feedback control action can still be carried on for those unaffected controllers. To validate this claim, we consider some scenarios where one or some of the local controllers are damaged. Through simulations, we show that for certain cases, adequate closed-loop responses can still be maintained.

TABLE III
MULTIPLE LOAD CHANGES

Scenarios	Area 1	Area 2	Area 3	Area 4
B_1- Original	0.1	0	0	0
B_2	0.1	0.2	0.2	0.1
B_3	0.2	0.1	0.1	0.2

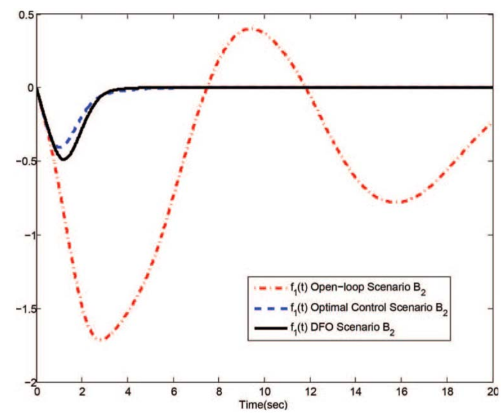

Fig. 13. $f_1(t)$ responses to multiple load changes in scenario B_2.

TABLE IV
FAULTS ANALYSIS

Scenarios	Areas under attacked	Impacts on the system
C_1	Area 2	$\hat{u}_2(t) = 0$
C_2	Areas $2, 3$	$\hat{u}_2(t) = 0$, $\hat{u}_3(t) = 0$
C_3	Areas $2, 3, 4$	$\hat{u}_k(t) = 0, k \in (2, 3, 4)$

Table IV tabulates three scenarios where some of the local controllers of the four-area interconnected power system are damaged. Thus, for instance, say for scenario C_2, the local controllers of areas 2 and 3 are damaged and as a result, the control signals $\hat{u}_2(t) = 0$ and $\hat{u}_3(t) = 0$ are not available for feedback control. A simulation test is then undertaken to verify the effectiveness of our DFO scheme in comparison to a CO-based control scheme such as the well-known LRO scheme. Note that, when a centralized control facility is damaged, all the control signals are unavailable and hence the performance of the system in this circumstance is in fact the open-loop performance.

Figs. 14 and 15 show the responses of $f_1(t)$ and $P_{\text{tie},1}(t)$ for the three scenarios where a 0.1 p.u. step load change occurs at area 1. It is observed that when load disturbances happen at area 1 (which is not damaged in all of the considered scenarios), the action of the remaining controllers still provides adequate performance for $f_1(t)$ and $P_{\text{tie},1}(t)$ as their fluctuations can be brought back to zeros.

In addition, Fig. 16 shows the responses of $f_1(t)$ for the three scenarios where now a step load change occurs at area 3 and also at area 4. Since load disturbances happen at areas 3 and 4 (which are damaged as depicted in scenarios C_2 and C_3), we can see that $f_1(t)$ cannot be brought back to zero for scenarios C_2 and C_3. Nevertheless, its steady-state is now brought closer to zero and its responses are less fluctuated when compared to the open-loop situation.

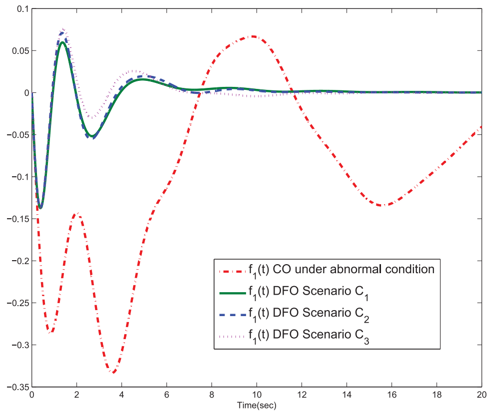

Fig. 14. $f_1(t)$ responses to a 0.1 p.u. step load change at area 1.

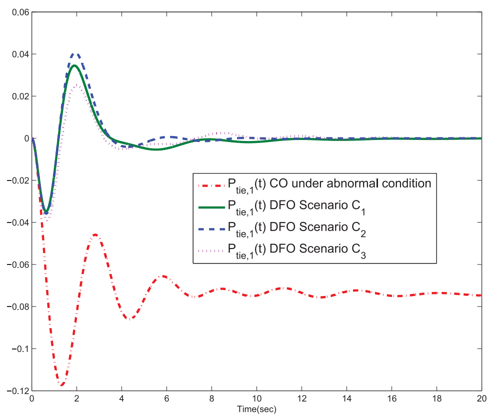

Fig. 15. $P_{\mathrm{tie},1}(t)$ responses to a 0.1 p.u. step load change at area 1.

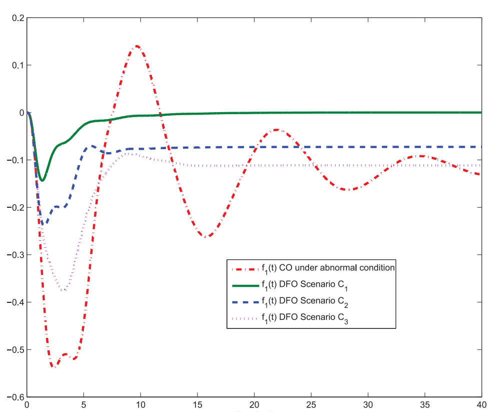

Fig. 16. $f_1(t)$ responses to a 0.1 p.u. step load change at areas 3 and 4.

Remark 3: The results developed in this paper generalizable for general power system topologies with a large number of interconnected areas. To validate this point, we have undertaken some further studies on five- and six-area interconnected power systems with a variety of links. Their topologies are shown in Figs. 17 and 18. Now, based on Section II, we can readily obtain a mathematical model for the five-area and six-area power systems with 38 and 47 state variables, respectively. By the same method of design and analysis, we can design DFOs for the two considered systems. The results are

TABLE V
MINIMUM ORDER OBSERVER ANALYSIS

Five-area power system				
No. of states	No. of outputs	LRO centralized scheme observer order	CFO centralized scheme observer order	DFO distributed scheme observer order
38	24	14	5	2
Six-area power system				
No. of states	No. of outputs	LRO centralized scheme observer order	CFO centralized scheme observer order	DFO distributed scheme observer order
47	29	18	7	2

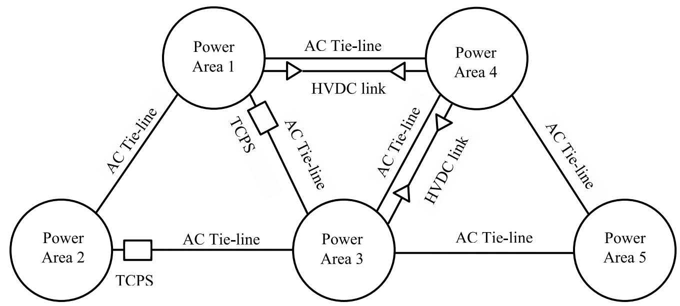

Fig. 17. Block diagram representation of a five-area power system.

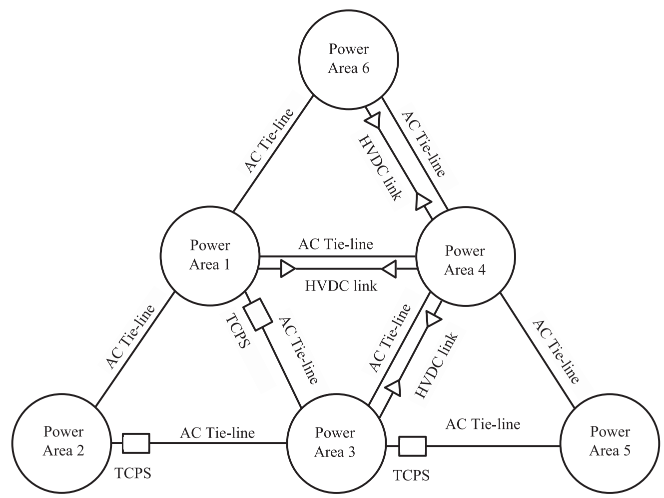

Fig. 18. Block diagram representation of a six-area power system.

tabulated in Table V. In all cases, a second-order DFO can be readily designed for each power area.

Figs. 19–22 show the responses of $f_1(t)$ and $P_{\mathrm{tie},1}(t)$ for the two systems when a 0.1 p.u. step load change occurs at area 1. It is clear that the closed-loop performance of the systems under the proposed distributed control scheme is satisfactory.

Remark 4: It is envisaged that the design method of this paper can be extended to wider classes of systems that include nonlinearities and/or uncertainties. For instance, consider the following system:

$$\begin{aligned}\dot{x}(t) &= Ax(t) + Bu(t) + f((x,u),y) + \Gamma d(t)\\ y(t) &= Cx(t)\end{aligned} \tag{30}$$

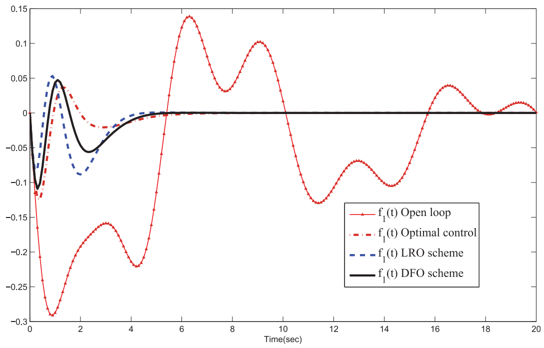

Fig. 19. $f_1(t)$ responses to a 0.1 p.u. step load change at area 1 (five-area power system).

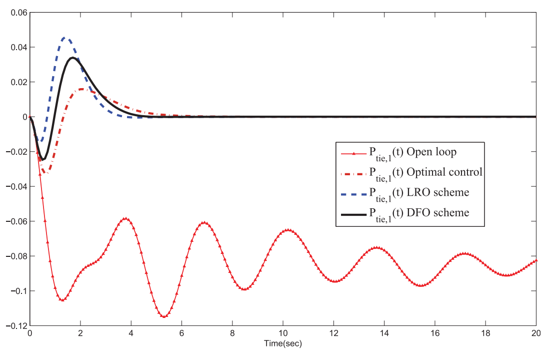

Fig. 20. $P_{\text{tie},1}(t)$ responses to a 0.1 p.u. step load change at area 1 (five-area power system).

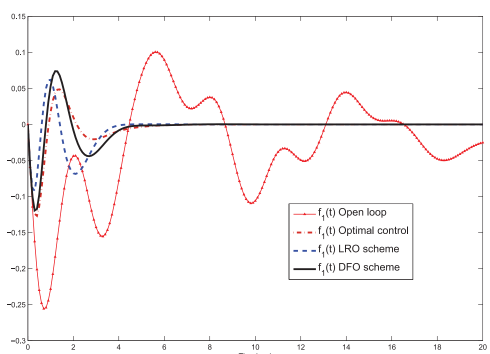

Fig. 21. $f_1(t)$ responses to a 0.1 p.u. step load change at area 1 (six-area power system).

where $f((x, u), y)$ is a real nonlinear vector function on $\mathbb{R}^n$. As discussed in [33], by decomposing the nonlinear function $f(.,.)$ into two parts: 1) a nonlinear part comprises a Lipschitz nonlinear function with respect to the state and input; and 2) a state-dependent unknown part including state/input uncertainties, time-varying terms, additive disturbance, etc. Based on the method of this paper, we can extend the design to nonlinear cases. In such case, the structure of the observer (14) needs to be modified to include some extra terms in order to counteract the nonlinear function. Also, we may need to resort to some efficient linear matrix inequality-based techniques in order to analyze the asymptotic stability of the error system. Some preliminary works have been reported in [33].

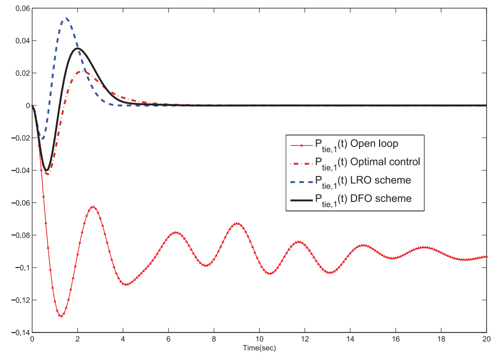

Fig. 22. $P_{\text{tie},1}(t)$ responses to a 0.1 p.u. step load change at area 1 (six-area power system).

However, this is a challenging topic and therefore we would like to leave it for future research work.

Remark 5: In this paper, we assume that there is enough EVs which are plug-in to the grid so that their contribution to LFC is smaller than their capacity which means that there is still enough reserve left in their batteries. Thus, under this assumption and as we have already demonstrated, EVs were able to provide their share of 10% and therefore fully participated in the LFC to meet the load demand. In such case, we only need 90% contribution from the thermal plant. On the other hand, when this assumption is not met and also due to the stochastic nature of EVs (i.e., from plugging-in and plugging-out), it is important to analyze the robustness of our proposed DFO scheme.

For this, we conducted a number of tests. Firstly, we tested the robustness of our DFO scheme under a scenario (scenario D_1) where the contribution of EVs is not available. Thus, in this situation, EVs are not participated altogether in the LFC scheme, and this implies that in the block-diagram of Fig. 1, we have $\alpha_{ei} = 0$ and $P_{ei}(t) = 0$, $i = 1, 2, 3, 4$. As a result, the augmented closed-loop system (26) is reduced to an augmented closed-loop system with a smaller dimension due to $\alpha_{ei} = 0$ and $P_{ei}(t) = 0$, $i = 1, 2, 3, 4$. Using the same parameters of the DFOs designed for the un-faulted situation, we found that the new augmented closed-loop system is stable and our DFO scheme still able to main the frequency and interchange power deviations with zero steady-state values. Note that when the EVs are not available, the power plant takes over and provides the required load demand. We have undertaken extensive simulations to test this worst case scenario. For illustrative purpose, Figs. 23 and 24 show the responses of $P_{g1}(t)$, $P_{e1}(t)$, and $f_1(t)$ to a 0.1 p.u. step load change at area 1 under a faulty situation where during the time intervals from 10 to 20 s and 30 to 50 s, EVs were not available altogether. It is clear from these figures that $f_1(t)$ converges to zero steady-state value and that whenever EVs are not available, the power plant takes over and provides the required load demand. This analysis shows that our proposed DFO scheme is robust and effective in coping with faulty situations.

In our next test, we considered a scenario (scenario D_2) where in addition to loosing all of the EVs at some time intervals (i.e., scenario D_1), we also have EVs being subjected to stochastic fluctuations due to them being plugging-in and out

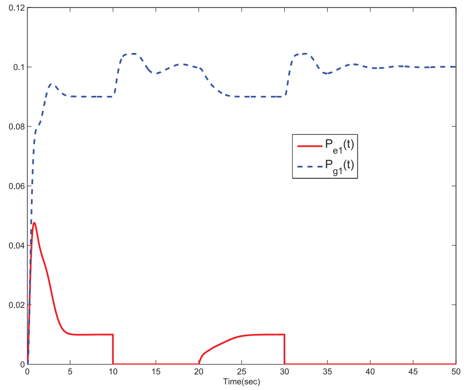

Fig. 23. Responses of $P_{g1}(t)$ and $P_{e1}(t)$ to a 0.1 p.u. step load change at area 1 under scenario D_1.

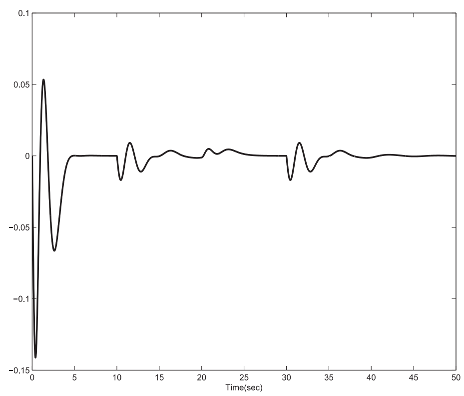

Fig. 24. Response of $f_1(t)$ to a 0.1 p.u. step load change at area 1 under scenario D_1.

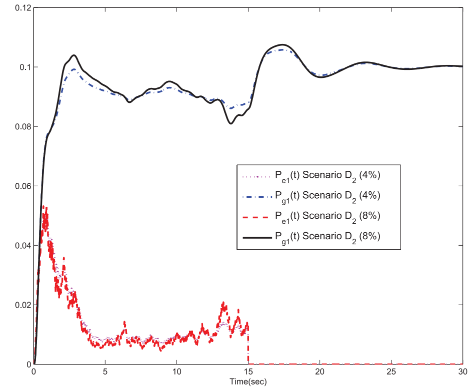

Fig. 25. Responses of $P_{g1}(t)$ and $P_{e1}(t)$ to a 0.1 p.u. step load change at area 1 under scenario D_2.

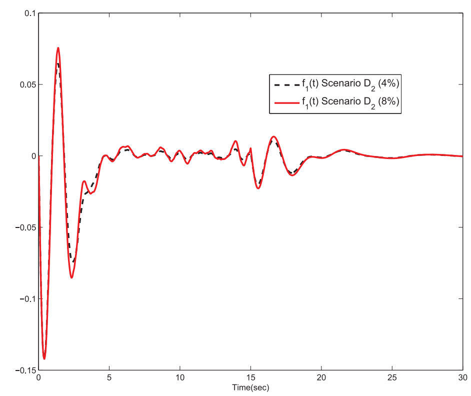

Fig. 26. Response of $f_1(t)$ to a 0.1 p.u. step load change at area 1 under scenario D_2.

of the grid. In this test, we simulated two cases depicting some realistic situations where the power output of EVs is subjected to random fluctuations of 4% and 8% from its nominal value and that the fluctuations occur within a very fast time interval of 0.01 s for a duration of 15 s. Figs. 25 and 26 show the responses of $P_{g1}(t)$, $P_{e1}(t)$, and $f_1(t)$ to a 0.1 p.u. step load change at area 1 under this scenario. As expected, due to random fluctuations of EVs, the steady-state value of $f_1(t)$ cannot be exactly zero, but it is still within an acceptable value as there is a small magnitude of fluctuations around zero. Also, $f_1(t)$ has a larger magnitude of fluctuations when there is a larger change in the output of EVs.

Finally, in our last test, we considered a possible research direction in order to improve the robustness of the closed-loop system. For this, we compared the performance of our designed DFOs for two optimal state feedback controllers designed under scenarios A_1 and A_4. Note that in scenario A_4, α was changed from -1 to -0.3 and that it has a longer settling time than in scenario A_1. Extensive simulations have been undertaken to test the performance of both controllers for various random fluctuations in the power output of EVs. For illustrative purpose, Fig. 27 shows the responses of $f_1(t)$ for the case where there was an 8% fluctuations in the power output of EVs for both controllers. It is observed that the designed DFO for scenario A_1 can handle the fluctuations better than scenario A_4 as the magnitude of fluctuations is smaller. This paper suggests that there is a possible way to improve the performance of the closed-loop system to better handle the stochastic nature of EVs. However, this calls for a deeper research into the topic and it is beyond the scope of this paper. We therefore would like further research to be carried out to address this very important research question in dealing with random stochastic of EVs.

Remark 6: In this remark, we discuss the robustness of our DFO-based controller scheme to time delays. With regard to our DFO-based controller scheme, at each local area (i.e., the ith area), the estimated control signal, $\hat{u}_i(t)$, is computed according to (24) and (25). Here, $y_a^i(t)$ comprises local output, $y_i(t)$, and additional outputs from the other remote areas, $y_r^i(t)$. The implementation of the control signal $\hat{u}_i(t)$ is as shown in Fig. 7. It is clear that, $y_r^i(t)$ is required to be sent over to the ith area in order to realize the estimated feedback control signal. In most cases, the measurement data, $y_r^i(t)$, is transmitted through a communication channel and thus time delays will arise. At a particular area, information exchange from its distant areas may encounter distinct latencies, depending on the distance between the transmitting and receiving ends, the magnitude of data traffics and the bandwidth of the communication channels. Such a time delay is designated by the term $\tau_{ji}(t) > 0$ with j representing the identifier of the interconnected area where the information is originated from.

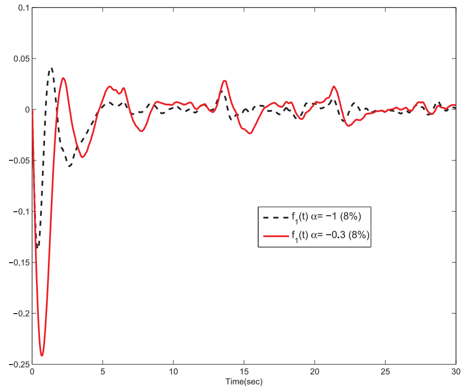

Fig. 27. Responses of $f_1(t)$ to a 0.1 p.u. step load change at area 1 with 8% random fluctuations in EVs.

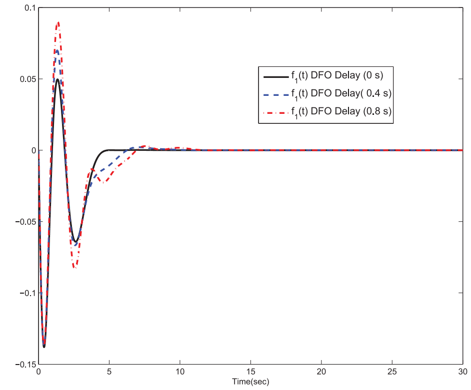

Fig. 28. Responses of $f_1(t)$ to a 0.1 p.u. step load change at area 1 with time delays in the outputs.

More precisely, let us now turn our attention to Fig. 7. Due to these time delays, $y_r^1(t)$ now cannot have instantaneous outputs information from areas 2, 3, 4. Instead, it now comprises the following delayed outputs information $y_2^1(t - \tau_{21}(t)) + y_3^1(t - \tau_{31}(t)) + y_4^1(t - \tau_{41}(t))$. In a similar manner, the estimated control signals for the rest of the areas ($i = 2, 3, 4$) are also subjected to time delays. As a result, the augmented closed-loop system (26) contains multiple time-varying delays and as such its closed-loop stability will not always be ensured due to the presence of these time delays. In this regard, it is still possible to analyze the closed-loop stability of the augmented closed-loop system and derive some upper bounds for the time-varying delays in order to ensure stability of the overall system. This is a subject for future research papers and it is not our scope to address it in this paper due to the page limitation of a journal paper.

It should be noted here that our DFO scheme is more robust to time delays than conventional centralized reduced-order Luenberger observer scheme. For this, we undertook extensive simulations to test the robustness of our DFO scheme for the cases where there are multiple time-varying delays and they vary within different intervals, i.e., $0 < \tau_{ji}(t) < \tau_{\max}$. For illustrative purpose, Fig. 28 shows the responses of $f_1(t)$ for two cases where the delays vary within 0.4 and 0.8 s for all $i, j = 1, 2, 3, 4$. It is clear that time delays have effected the closed-loop system performance, however, despite this, the system is still stable and that the steady-state values of $f_1(t)$ still converge to zero. On the other hand, for centralized reduced-order Luenberger observer schemes, they are very vulnerable to time delays. Since to implement such a scheme, it requires a central facility. For the sake of comparison, let us assume that the central facility is located at area 1. Therefore, as explained above, the outputs information from areas 2, 3, 4 are needed to be sent over to area 1 and this gives rise to time delays in the closed-loop system. We have also undertook simulation for two cases where the delays are at 0.4 and 0.8 s and found that for both cases, centralized reduced-order Luenberger observer scheme failed to maintain closed-loop system stability.

Remark 7: In Section I, we explained that an open communication infrastructure is necessary in order to integrate EVs into the smart grid. To simplify the problem at hand, we assumed that the communication happens at a very high speed relative to the speed of the closed-loop system and therefore we ignored any network-induced communication delay that may arise in the communication channel. As a result, the model shown in Fig. 1 does not contain a time delay in the path from P_{ci} to P_{ei}. Such an assumption is reasonable as it is justifiable by analyzing the robustness of our DFO scheme when it is subjected to time delays in the control input. Accordingly, in the following analysis, we consider the case where a network-induced delay, $\tau(t)$, actually exists in the transmission channel. Fig. 29 now shows a modified block diagram of a general transfer function model of N-area interconnected power.

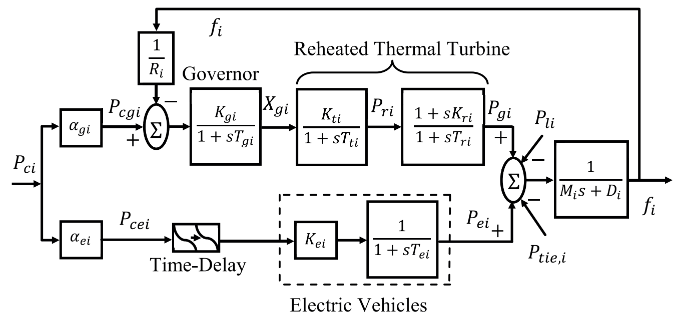

Fig. 29. Transfer function model of N-area interconnected power system with an input time-delay, $\tau(t)$.

In our robustness analysis, we undertook extensive simulations to test the performance of our DFO scheme for various situations where network-induced communication delays are constant and also time-varying within an interval, i.e., $0 < \tau(t) \leq \tau_m$. We also undertook simulations to compare the performance of our DFO scheme against those centralized schemes (i.e., CFO and LRO) where they were also subjected to the same time delays. For illustrative purpose, we analyze the robustness of DFO, CFO, and LRO schemes for the case as tabulated in the first row of Table I. Fig. 30 shows the responses of the frequency deviation $f_1(t)$ to a 0.1 p.u. step load change at area 1 with different time delays of $\tau(t) = 0.1$ s, $\tau(t) = 0.2$ s, and $\tau(t) = 0.1 + 0.2|\sin(t)|$. It is clear from Fig. 30 that our DFO scheme is robust against time delays in the communication channel. Notably, when the delays are

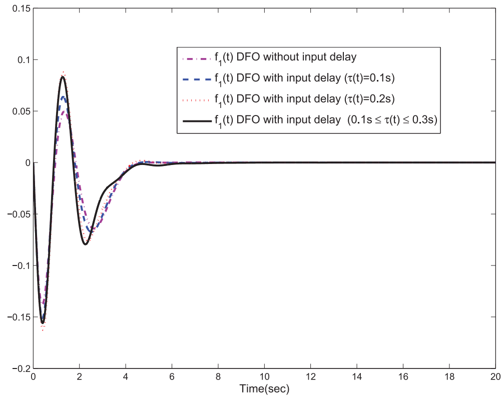

Fig. 30. $f_1(t)$ responses to a 0.1 p.u. step load change at area 1 with input time delays.

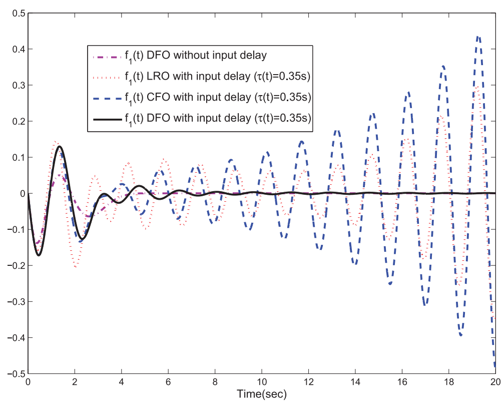

Fig. 31. $f_1(t)$ responses to a 0.1 p.u. step load change at area 1 with input time delays.

small, the responses of $f_1(t)$ are comparable to the response of $f_1(t)$ for the case where there is no time delay. This fact therefore justifies our assumption to ignore communication delays in the channel. Since for small time delays, their impacts on the performance of the closed-loop system are not that detrimental.

It is also worthwhile to point out that our DFO scheme is more robust than the centralized schemes (CFO and LRO). Indeed, Fig. 31 shows the responses of $f_1(t)$ for the case where a sizable time delay of $\tau(t) = 0.35$ s occurred in the communication channel. It is clear from the figure that both centralized schemes, CFO and LRO, cannot cope with such a time delay as their closed-loop systems are unstable and resulted in unacceptable responses. Whereas, our designed DFO scheme still provides satisfactory response as $f_1(t)$ converges to zeros after a step load disturbance. This fact highlights another advantage of our DFO scheme over that of centralized schemes.

In summary, with extensive analysis and evaluation through Remarks 1–7, we have demonstrated the capability of our proposed DFO scheme.

V. Conclusion

This paper has presented a novel LFC scheme using EVs to provide the stability fluctuated by load demands. First, a general framework for deriving a state-space model for general power system topologies with a large number of connected areas has been given. Based on this general framework, a detailed model of a four-area power system incorporating a smart, renewable discharged EVs system and diverse transmission links has been considered. LFC has been studied based on a novel application of functional observers. Novel reduced-order DFOs have been designed, one at each local area, to implement any given global state feedback controller. The proposed scheme can cope better against accidental failures and more robust than conventional CO-based controller schemes. Extensive simulations and comparisons have been given to show the effectiveness of the proposed control scheme.

Appendix A

The matrix A_{ii} in (11) for $i \in \{1, 2, 3, 4\}$ can be partitioned as $A_{ii} = \begin{bmatrix} A_{ii,a} & A_{ii,b} \\ A_{ii,c} & A_{ii,d} \end{bmatrix}$, where $A_{ii,a} \in \mathbb{R}^{6\times 6}$, $A_{ii,b} \in \mathbb{R}^{6\times(n_i-6)}$, $A_{ii,c} \in \mathbb{R}^{(n_i-6)\times 6}$, and $A_{ii,d} \in \mathbb{R}^{(n_i-6)\times(n_i-6)}$. Matrices $A_{ii,a}$ for $i \in \{1, 2, 3, 4\}$ is expressed as

$$A_{ii,a} = \begin{bmatrix} -\frac{D_i}{M_i} & 0 & 0 & \frac{1}{M_i} & \frac{1}{M_i} & 0 \\ \beta_{1i} & -\frac{1}{T_{gi}} & 0 & 0 & 0 & 0 \\ 0 & \beta_{2i} & -\frac{1}{T_{ti}} & 0 & 0 & 0 \\ 0 & \beta_{3i} & \beta_{4i} & -\frac{1}{T_{ri}} & 0 & 0 \\ 0 & 0 & 0 & 0 & -\frac{1}{T_{ei}} & 0 \\ b_i & 0 & 0 & 0 & 0 & 0 \end{bmatrix} \quad (31)$$

and $\beta_{1i} = -(K_{gi}/R_iT_{gi})$, $\beta_{2i} = (K_{ti}/T_{ti})$, $\beta_{3i} = (K_{ti}K_{ri}/T_{ti}T_{ri})$, $\beta_{4i} = (T_{ti} - K_{ri})/T_{ti}T_{ri}$. $A_{11,b} \in \mathbb{R}^{6\times 3}$, $A_{11,c} \in \mathbb{R}^{3\times 6}$, $A_{11,d} \in \mathbb{R}^{3\times 3}$, $A_{22,b}, A_{33,b} \in \mathbb{R}^{6\times 2}$, $A_{22,c}, A_{33,c} \in \mathbb{R}^{2\times 6}$, $A_{22,d}, A_{33,d} \in \mathbb{R}^{2\times 2}$ are given as

$$A_{11,b} = \begin{bmatrix} -\dfrac{1}{M_1} & 0 & 0 \\ 0_{4\times 1} & 0_{4\times 1} & 0_{4\times 1} \\ 1 & 0 & 0 \end{bmatrix}, \quad A_{11,c} = \begin{bmatrix} \Psi_1 & 0_{1\times 5} \\ \dfrac{K_{14}}{T_{\mathrm{dc}1}} & 0_{1\times 5} \\ \dfrac{K_{s13}}{T_{s13}} & 0_{1\times 5} \end{bmatrix}$$

$$A_{11,d} = \begin{bmatrix} 0 & -\dfrac{1}{T_{\mathrm{dc}1}} & -\dfrac{1}{T_{s13}} \\ 0 & -\dfrac{1}{T_{\mathrm{dc}1}} & 0 \\ 0 & 0 & -\dfrac{1}{T_{s13}} \end{bmatrix}, \quad A_{22,b} = \begin{bmatrix} -\dfrac{1}{M_2} & 0 \\ 0_{4\times 1} & 0_{4\times 1} \\ 1 & 0 \end{bmatrix}$$

$$\Psi_1 = 2\pi(T_{12} + T_{13} + T_{14}) + T_{13}\frac{K_{s13}}{T_{s13}} + \frac{K_{14}}{T_{\mathrm{dc}1}}$$

$$A_{22,c} = \begin{bmatrix} \Psi_2 & 0_{1\times 5} \\ T_{23}\dfrac{K_{s23}}{T_{s23}} & 0_{1\times 5} \end{bmatrix}, \quad A_{22,d} = \begin{bmatrix} 0 & -\dfrac{1}{T_{s23}} \\ 0 & -\dfrac{1}{T_{s23}} \end{bmatrix}$$

$$\Psi_2 = 2\pi(T_{21} + T_{23}) + T_{23}\frac{K_{s23}}{T_{s23}}$$

$$A_{33,b} = \begin{bmatrix} -\dfrac{1}{M_3} & 0 \\ 0_{4\times 1} & 0_{4\times 1} \\ 1 & 0 \end{bmatrix}, \quad A_{33,d} = \begin{bmatrix} 0 & -\dfrac{1}{T_{\mathrm{dc}3}} \\ 0 & -\dfrac{1}{T_{\mathrm{dc}3}} \end{bmatrix}$$

$$A_{33,c} = \begin{bmatrix} \Psi_3 & 0_{1\times 5} \\ \dfrac{K_{34}}{T_{\mathrm{dc}3}} & 0_{1\times 5} \end{bmatrix}, \Psi_3 = 2\pi(T_{31} + T_{32} + T_{34}) + \frac{K_{34}}{T_{\mathrm{dc}3}}.$$

$A_{44} = A_{ii,a} \in \mathbb{R}^{6\times6}$ in (31) with $i = 4$, and matrices $A_{44,b}$, $A_{44,c}$, $A_{44,d}$ are [Ø]. Matrices A_{ij} in (11) are partitioned as $A_{ij} = \begin{bmatrix} A_{ij,a} \\ A_{ij,b} \end{bmatrix}$, where $A_{ij,a} \in \mathbb{R}^{6\times n_j}$ are null matrices, $A_{ij,b} \in \mathbb{R}^{(n_i-6)\times n_j}$, and n_i, n_j are number of state variables of power area i and j for $i \in \{1, 2, 3\}$ and $j \in \{1, 2, 3, 4\}, j \neq i$. Matrices $A_{ij,b}$ are given at the following:

$$A_{12,b} = \begin{bmatrix} -2\pi T_{12} & 0_{1\times7} \\ 0_{2\times1} & 0_{2\times7} \end{bmatrix},\ A_{13,b} = \begin{bmatrix} -2\pi T_{13} & 0_{1\times7} \\ 0_{2\times1} & 0_{2\times7} \end{bmatrix}$$

$$A_{14,b} = \begin{bmatrix} -2\pi T_{14} - \dfrac{K_{14}}{T_{\mathrm{dc1}}} & 0_{1\times5} \\ -\dfrac{K_{14}}{T_{\mathrm{dc1}}} & 0_{1\times5} \\ 0 & 0_{1\times5} \end{bmatrix},\ A_{24,b} = 0_{2\times6}$$

$$A_{21,b} = \begin{bmatrix} -2\pi T_{21} & 0_{1\times8} \\ 0 & 0_{1\times8} \end{bmatrix},\ A_{23,b} = \begin{bmatrix} -2\pi T_{23} & 0_{1\times7} \\ 0 & 0_{1\times7} \end{bmatrix}$$

$$A_{31,b} = \begin{bmatrix} -2\pi T_{31} - \dfrac{K_{s13}}{T_{s13}} T_{13} & 0_{1\times7} & \dfrac{1}{T_{s13}} \\ 0 & 0_{1\times7} & 0 \end{bmatrix}$$

$$A_{32,b} = \begin{bmatrix} -2\pi T_{32} - \dfrac{K_{s23}}{T_{s23}} T_{23} & 0_{1\times6} & \dfrac{1}{T_{s23}} \\ 0 & 0_{1\times6} & 0 \end{bmatrix}$$

$$A_{34,b} = \begin{bmatrix} -2\pi T_{34} - \dfrac{K_{34}}{T_{\mathrm{dc3}}} & 0_{1\times5} \\ -\dfrac{K_{34}}{T_{\mathrm{dc3}}} & 0_{1\times5} \end{bmatrix}.$$

Matrix A_{ij} with $i = 4$ such as $A_{41} \in \mathbb{R}^{6\times9}, A_{42}, A_{43} \in \mathbb{R}^{6\times8}$ are expressed at the following:

$$A_{41} = \begin{bmatrix} 0_{1\times6} & \dfrac{1}{M_4} & 0_{1\times2} \\ 0_{4\times6} & 0 & 0_{4\times2} \\ 0_{1\times6} & -1 & 0_{1\times2} \end{bmatrix}$$

$$A_{42} = A_{43} = \begin{bmatrix} 0_{1\times6} & \dfrac{1}{M_4} & 0 \\ 0_{4\times6} & 0_{4\times1} & 0_{4\times1} \\ 0_{1\times6} & -1 & 0 \end{bmatrix}.$$

The matrices $B_i \in R^{n_i}$ and $\Gamma_i \in R^{n_i}$ are given as

$$B_i = \begin{bmatrix} 0 & \alpha_{gi}\dfrac{K_{gi}}{T_{gi}} & 0 & 0 & \alpha_{ei}\dfrac{K_{ei}}{T_{ei}} & 0_{1\times(n_i-5)} \end{bmatrix}^T$$

$$\Gamma_i = \begin{bmatrix} -\dfrac{1}{M_i} & 0_{1\times(n_i-1)} \end{bmatrix}^T.$$

Appendix B

The data for proposed system is collected following [1], [2], [8], [11], [24], [39]:

$$T_{ti} = 0.3, K_{ti} = 1, K_{ri} = 0.5, T_{ri} = 10, K_{gi} = 1, T_{gi} = 0.08$$
$$R_i = 2.4\ , K_{ei} = 1, T_{ei} = 1, \alpha_{gi} = 0.9,\ \alpha_{ei} = 0.1$$
$$M_i = 0.1667, b_i = 0.4250, D_i = 0.0083, T_{ij} = T_{ji} = 0.0260$$
$$2\pi T_{ij} = 0.1634, K_{14} = K_{34} = 0.1, T_{\mathrm{dc1}} = T_{\mathrm{dc3}} = 0.2$$
$$K_{s13} = K_{s23} = 1, T_{s13} = T_{s23} = 0.1.$$

The optimal control $u(t) = Fx(t)$ in (10) is designed to minimize the cost function $J_u = \int_0^\infty (x^T(t)Qx(t) + u^T(t)Ru(t))dt$, where $Q \geq 0$ and $R > 0$ are state cost weighting matrix and control cost weighting matrix, respectively. The control law is computed by solving the Riccati equation $A^TP + PA - PBR^{-1}B^TP + Q = 0$ (see [32]). Using LQR design with $Q = I_{31}$, $R = I_4$ and also by imposing all the closed-loop poles of the system (11) to have prescribed stability of at least $\alpha = -1$ [MATLAB command lqr$(A + I_{31}, B, Q, R)$], an optimal state feedback control gain, F, is easily obtained, where

$$F = \begin{bmatrix} F_1 \\ F_2 \\ F_3 \\ F_4 \end{bmatrix} = \begin{bmatrix} F_{11} & F_{12} & F_{13} & F_{14} \\ F_{21} & F_{22} & F_{23} & F_{24} \\ F_{31} & F_{32} & F_{33} & F_{34} \\ F_{41} & F_{42} & F_{43} & F_{44} \end{bmatrix}.$$

References

[1] H. Bevrani, *Robust Power System Frequency Control*. New York, NY, USA: Springer, 2009.

[2] P. Kundur, *Power System Stability and Control*. New York, NY, USA: McGraw-Hill, 1994.

[3] M. Aldeen and H. Trinh, "Load frequency control of interconnected power systems via constrained feedback control schemes," *Int. J. Comput. Elect. Eng.*, vol. 20, no. 1, pp. 71–88, Jan. 1994.

[4] I. Ibraheem, P. Kumar, and D. P. Kothari, "Recent philosophies of automatic generation control strategies in power systems," *IEEE Trans. Power Syst.*, vol. 20, no. 1, pp. 346–357, Feb. 2005.

[5] S. K. Pandey, S. R. Mohanty, and N. Kishor, "A literature survey on load-frequency control for conventional and distribution generation power systems," *Renew. Sustain. Energy Rev.*, vol. 25, pp. 318–334, Sep. 2013.

[6] A. Sarlette, J. Dai, Y. Phulpin, and D. Ernst, "Cooperative frequency control with a multi-terminal high-voltage DC network," *Automatica*, vol 48, no. 12, pp. 3128–3134, Dec. 2012.

[7] K. S. Vijay, *HVDC and FACTS Controllers*. Boston, MA, USA: Kluwer Academic, 2004.

[8] Ibraheem, Nizamuddin, and T. S. Bhatti, "AGC of two area power system interconnected by AC/DC links with diverse sources in each area," *Int. J. Elect. Power Energy Syst.*, vol. 55, pp. 297–304, Feb. 2014.

[9] E. Rakhshani, A. Luna, K. Rouzbehi, P. Rodriguez, and I. Etxeberria-Otadui, "Effect of VSC-HVDC on load frequency control in multi-area power system," in *Proc. IEEE Energy Convers. Congr. Expo.*, Raleigh, NC, USA, 2012, pp. 4432–4436.

[10] S. Bhamidipati and A. Kumar, "Load frequency control of an interconnected system with DC tie-lines and AC-DC parallel tie-lines," in *Proc. 22nd Annu. North Amer. Power Symp.*, Auburn, AL, USA, 1990, pp. 390–395.

[11] R. J. Abraham, D. Das, and A. Patra, "Effect of TCPS on oscillations in tie-power and area frequencies in an interconnected hydrothermal power system," *IET Gener. Transm. Distrib.*, vol. 1, no. 4, pp. 632–639, Jul. 2007.

[12] K. Xing and G. Kusic, "Application of thyristor-controlled phase shifters to minimize real power losses and augment stability of power systems," *IEEE Trans. Energy Convers.*, vol. 3, no. 4, pp. 792–798, Dec. 1988.

[13] M. Yilmaz and P. T. Krein, "Review of the impact of vehicle-to-grid technologies on distribution systems and utility interfaces," *IEEE Trans. Power Electron.*, vol. 28, no. 12, pp. 5673–5689, Dec. 2013.

[14] H. Yang, C. Y. Chung, and J. Zhao, "Application of plug-in electric vehicles to frequency regulation based on distributed signal acquisition via limited communication," *IEEE Trans. Power Syst.*, vol. 28, no. 2, pp. 1017–1026, May 2013.

[15] M. Yilmaz and P. T. Krein, "Review of battery charger topologies, charging power levels, and infrastructure for plug-in electric and hybrid vehicles," *IEEE Trans. Power Electron.*, vol. 28, no. 5, pp. 2151–2169, May 2013.

[16] C. Guille and G. Gross, "A conceptual framework for the vehicle-to-grid (V2G) implementation," *Energy Policy*, vol. 37, no. 11, pp. 4379–4390, Nov. 2009.

[17] H. Liu, Z. Hu, Y. Song, and J. Lin, "Decentralized vehicle-to-grid control for primary frequency regulation considering charging demands," *IEEE Trans. Power Syst.*, vol. 28, no. 3, pp. 3480–3489, Aug. 2013.

[18] Y. Mu, J. Wu, J. Ekanayake, N. Jenkins, and H. Jia, "Primary frequency response from electric vehicles in the Great Britain power system," *IEEE Trans. Smart Grid*, vol. 4, no. 2, pp. 1142–1150, Jun. 2013.

[19] Y. Ota *et al.*, "Autonomous distributed V2G (vehicle-to-grid) satisfying scheduled charging," *IEEE Trans. Smart Grid*, vol. 3, no. 1, pp. 559–564, Mar. 2012.
[20] S. Vachirasricirikul and I. Ngamroo, "Robust LFC in a smart grid with wind power penetration by coordinated V2G control and frequency controller," *IEEE Trans. Smart Grid*, vol. 5, no. 1, pp. 371–380, Jan. 2014.
[21] M. Takagi, K. Yamaji, and H. Yamamoto, "Power system stabilization by charging power management of plug-in hybrid electric vehicles with LFC signal," in *Proc. Veh. Power Propul. Conf.*, Dearborn, MI, USA, 2009, pp. 822–826.
[22] W. Kempton and J. Tomić, "Vehicle-to-grid power implementation: From stabilizing the grid to supporting large-scale renewable energy," *J. Power Sources*, vol. 144, no. 1, pp. 280–294, Jun. 2005.
[23] T. Masuta and A. Yokoyama, "Supplementary load frequency control by use of a number of both electric vehicles and heat pump water heaters," *IEEE Trans. Smart Grid*, vol. 3, no. 3, pp. 1253–1262, Sep. 2012.
[24] J. R. Pillai and B. Bak-Jensen, "Integration of vehicle-to-grid in the western Danish power system," *IEEE Trans. Sustain. Energy*, vol. 2, no. 1, pp. 12–19, Jan. 2011.
[25] H. Liu, Z. Hu, Y. Song, J. Wang, and X. Xie, "Vehicle-to-grid control for supplementary frequency regulation considering charging demands," *IEEE Trans. Power Syst.*, doi: 10.1109/TPWRS.2014.2382979.
[26] P. M. R. Almeida, J. A. P. Lopes, F. J. Soares, and M. H. Vasconcelos, "Automatic generation control operation with electric vehicles," in *Proc. iREP Symp. Bulk Power Syst. Dyn. Control (iREP)*, Rio de Janeiro, Brazil, 2010, pp. 1–7.
[27] D. Wu, D. C. Aliprantis, and L. Ying, "Load scheduling and dispatch for aggregators of plug-in electric vehicles," *IEEE Trans. Smart Grid*, vol. 3, no. 1, pp. 368–376, Mar. 2012.
[28] J. J. Escudero-Garzas, A. Garcia-Armanda, and G. Seco-Granados, "Fair design of plug-in electric vehicles aggregator for V2G regulation," *IEEE Trans. Veh. Technol.*, vol. 61, no. 8, pp. 3406–3419, Oct. 2012.
[29] E. L. Karfopoulos and N. D. Hatziargyriou, "A multi-agent system for controlled charging of a large population of electric vehicles," *IEEE Trans. Power Syst.*, vol. 28, no. 2, pp. 1196–1204, May 2013.
[30] M. D. Galus, S. Koch, and G. Andersson, "Provision of load frequency control by PHEVs, controllable loads, a cogeneration unit," *IEEE Trans. Ind. Electron.*, vol. 58, no. 10, pp. 4568–4582, Oct. 2011.
[31] K. Yamashita and T. Taniguchi, "Optimal observer design for load frequency control," *Int. J. Elect. Power Energy Syst.*, vol. 8, no. 2, pp. 93–100, Apr. 1986.
[32] M. Aldeen and J. F. Marsh, "Decentralised proportional-plus-integral design method for interconnected power systems," *Proc. Inst. Elect. Eng. Gener. Transm. Distrib.*, vol. 138, no. 4, pp. 263–274, Jul. 1991.
[33] H. Trinh and T. Fernando, *Functional Observers for Dynamical Systems*. Berlin, Germany: Springer, 2012.
[34] T. Fernando and H. Trinh, "A system decomposition approach to the design of functional observers," *Int. J. Control*, vol. 87, no. 9, pp. 1846–1860, 2014.
[35] T. L. Fernando, H. M. Trinh, and L. Jennings, "Functional observability and the design of minimum order linear functional observers," *IEEE Trans. Autom. Control*, vol. 55, no. 5, pp. 1268–1273, May 2010.
[36] L. S. Jennings, T. L. Fernando, and H. M. Trinh, "Existence conditions for functional observability from an eigenspace perspective," *IEEE Trans. Autom. Control*, vol. 56, no. 12, pp. 2957–2961, Dec. 2011.
[37] T. Fernando, S. MacDougall, V. Sreeram, and H. Trinh, "Existence conditions for unknown input functional observers," *Int. J. Control*, vol. 86, no. 1, pp. 22–28, Jan. 2013.
[38] H. Trinh, T. Fernando, H. H. C. Iu, and K. P. Wong, "Quasi-decentralized functional observers for the LFC of interconnected power systems," *IEEE Trans. Power Syst.*, vol. 28, no. 3, pp. 3513–3514, Aug. 2013.
[39] C. E. Fosha and O. I. Elgerd, "The megawatt-frequency control problem: A new approach via optimal control theory," *IEEE Trans. Power App. Syst.*, vol. PAS-89, no. 4, pp. 563–577, Apr. 1970.
[40] N. Rostamkolai *et al.*, "Control design of Santo Tome back-to-back HVDC link," *IEEE Trans. Power Syst.*, vol. 8, no. 3, pp. 1250–1256, Aug. 1993.
[41] J. Dai, Y. Phulpin, A. Sarlette, and D. Ernst, "Coordinated primary frequency control among non-synchronous systems connected by a multi-terminal high-voltage direct current grid," *IET Gener. Transm. Distrib.*, vol. 6, no. 2, pp. 99–108, Feb. 2012.

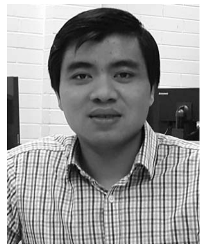

Thanh Ngoc Pham received the B.Eng. degree in electrical engineering with a major in automation and control from the Hanoi University of Science and Technology, Hanoi, Vietnam, in 2009, and the M.Eng. degree (Professional) in electrical and electronic engineering with a major in automation and control from Deakin University, Geelong, VIC, Australia, in 2013, where he is currently pursuing the Ph.D. degree with the Centre for Intelligent Systems Research.

His current research activities include power systems stability and control, time-delay systems, smart grid technology, and application of functional observers to load frequency control of interconnected power systems.

Hieu Trinh received the B.Eng. (Hons.), M.Eng.Sc., and Ph.D. degrees from the University of Melbourne, Melbourne, VIC, Australia, in 1990, 1992, and 1996, respectively, all in electrical and electronic engineering.

He began with Deakin University, Geelong, VIC, Australia, in 2001, where he is currently an Associate Professor. His current research interests include systems and control theory, fault diagnosis and fault-tolerant control, time-delay systems, and application of control theory to industrial systems and power systems. He has published a research book entitled *Functional Observers for Dynamical Systems* (Springer, 2012), and over 100 refereed journal papers on control engineering. He is very passionate about transferring/instilling his knowledge of control engineering to the next generation of engineers and Ph.D. researchers at Deakin University.

Prof. Trinh was a recipient of some national competitive research grants, such as Australian Research Council Grants, which allowed him to conduct his own research interests. He was a recipient of some recognitions for excellence in teaching from the offices of the Dean and Deputy Vice-Chancellor at Deakin University.

Le Van Hien received the B.Sc., M.Sc., and Ph.D. degrees from the Faculty of Mathematics and Informatics, Hanoi National University of Education, Hanoi, Vietnam, in 2001, 2004, and 2011, respectively, all in mathematics.

He is currently an Associate Professor in Mathematics with the Hanoi National University of Education. His current research interests include stability analysis and control of time-delay systems, state estimation and asymptotic behavior of dynamical systems, and control of complex systems, such as interconnected systems, hybrid systems, and H-infinity control.